PAPER

Design, fabrication, and testing of a low frequency MEMS piezoelectromagnetic energy harvester

To cite this article: Egon Fernandes *et al* 2018 *Smart Mater. Struct.* **27** 035017

View the article online for updates and enhancements.

Related content

- Finite element modeling of nonlinear piezoelectric energy harvesters with magnetic interaction
Deepesh Upadrashta and Yaowen Yang

- Design optimization of vibration energy harvesters fabricated by lamination of thinned bulk-PZT on polymeric substrates
Andrés Vásquez Quintero, Nadine Besse, Pattanaphong Janphuang et al.

- Modeling and design of Galfenol unimorph energy harvesters
Zhangxian Deng and Marcelo J Dapino

Design, fabrication, and testing of a low frequency MEMS piezoelectromagnetic energy harvester

Egon Fernandes[1], Blake Martin[1], Isabel Rua[2], Sid Zarabi[3], Hélène Debéda[2], David Nairn[3], Lan Wei[3] and Armaghan Salehian[4,5]

[1] Energy Harvesting and Vibrations Lab, Mechanical and Mechatronics Engineering, University of Waterloo, Waterloo, ON, N2L 3G1, Canada
[2] Université de Bordeaux, Laboratoire IMS, UMR 5218, Bordeaux INP, 351 Cours de la Libération, BAT A31, F-33405 Talence Cedex, France
[3] Electrical and Computer Engineering, University of Waterloo, Waterloo, ON, N2L 3G1, Canada
[4] Director of the Energy Harvesting and Vibrations Lab, Mechanical and Mechatronics Engineering, University of Waterloo, Waterloo, ON, N2L 3G1, Canada

E-mail: e22ferna@uwaterloo.ca, b6martin@uwaterloo.ca, maria-isabel.rua-taborda@u-bordeaux.fr, ssfarshc@uwaterloo.ca, helene.debeda@ims-bordeaux.fr, nairn@uwaterloo.ca, lan.wei@uwaterloo.ca and salehian@uwaterloo.ca

Abstract

This paper details a power solution for smart grid applications to replace batteries by harvesting the electromagnetic energy from a current-carrying wire. A MEMS piezoelectromagnetic energy harvester has been fabricated using PZT screen-printing technology with a centrally-supported meandering geometry. The energy harvesting device employs a symmetric geometry to increase its power output by reducing the effects of the torsional modes and the resultant overall strain nodes in the system subsequently reduce the complexities for the electrode fabrication. The unit is modelled using COMSOL to determine mode shapes and frequency response functions. A 12.7 mm by 14.7 mm unit is fabricated by screen-printing 75 μm-thick PZT on a stainless steel substrate and then experimentally tested to validate the FEA results. Experimentally, the harvester is shown to produce 9 μW from a wire carrying 7 A while operating at a distance of 6.5 mm from the wire. The design of the current work results in a greater normalized power density than other MEMS based piezoelectromagnetic devices and shows great potential relative to larger devices that use bulk or thin film piezoelectrics.

Keywords: smart materials, energy harvesting, piezoelectrics, smart grid

(Some figures may appear in colour only in the online journal)

1. Introduction

As the demand for electrical power increases, so does the strain on the aging power grid infrastructure. Continued use of electric components nearing failure has contributed to several major blackouts over the past decades. Electric utilities are modernizing their systems into a 'smart grid' that can detect critical changes through the use of sensors and wireless communications technology. Various sensors (current, temperature, etc) are also integrated into the smart grid to allow for monitoring of critical components. A vast number of sensors, distributed across the entire grid, are required to adequately monitor the system. Recent advancements in low-power electronics have created opportunities for wireless sensor nodes that combine sensors, power conditioning circuitry, and radios all into one small package and allow for remote sensing. These sensor nodes are typically powered by batteries that only have a lifespan of a few years. The cost to

replace these batteries can be immense as it involves both the battery and labor costs. Moreover, the installation of certain current sensors requires a power line to be disconnected and taken out of service causing disruptions to the given area. Considering these issues, there is a need to develop a non-invasive, low-cost, and self-powered solution for the sensor nodes.

Energy harvesting solutions that employ ambient or other sources of energy available to the system have proven as a viable option for powering electronics or wireless sensor nodes. Extensive research has been done in low-frequency electromagnetic vibration energy harvesting [1]. Previous work with piezoelectric cantilever beams has shown that both current sensing [2, 3] and energy harvesting [4, 5] are possible directly from AC conducting wires using non-invasive technology. The electromechanical vibration harvesting using bulk piezoelectric lead zirconate titanate (PZT) has been shown to produce better output than other comparable coil-based approaches where the harvester cannot encircle the conductor [6]. A Halbach array can also be used to focus the magnetic field to one side of the magnets and increase the electromagnetic force between the magnet array and the wire [7]. The piezoelectric solution can also be combined with other electromagnetic scavenging techniques to develop hybrid energy harvesters [8]. These AC energy harvesting solutions need to be scaled down to the micro-scale before becoming ubiquitous in the smart grid. Various micro-electromechanical system (MEMS) solutions allow for mass production that result in much smaller overall cost per unit. Screen-printing, for example, is a low cost additive process that allows for the creation of complex structures. Although a significant amount of literature deals with the screen-printing of PZT to form simple cantilever beams [9–12], little research has been performed regarding the same fabrication process for two-dimensional cantilevers (zigzag for instance) to create low frequency energy harvesters.

Migration to MEMS energy harvesting solutions also has some major hurdles. Piezoelectric cantilevers have been researched extensively for mechanical vibrations harvesting due to their simplicity [13]. For microsystems, however, cantilever beams tend to have a very high fundamental resonant frequency, which is not ideal for ambient energy harvesting where the available frequencies are low. This becomes problematic for energy harvesting from power lines as the harvester must be tuned to match the 60 Hz frequency of the current flow in the North American power grid.

Common methods to lower the fundamental frequency of a cantilever-based harvesting device include reducing the beam thickness, increasing the tip mass, or increasing the effective length of the beam. Most of these techniques become less practical when moving towards the micro-scale because of certain limitations regarding either quality or size. For example, while MEMS fabrications methods allow for piezoelectric thicknesses of about one micrometer, thin films typically have much weaker electromechanical properties than commercial bulk piezoelectrics and may not be suitable for energy harvesting applications. Also, the tip mass has limits due to size constraints of the packaging. Recently a

MEMS-scale cantilever was fabricated using aluminum nitride as the piezoelectric material [14]. Frequently, researchers increase the effective length of the system by using two-dimensional geometries. For instance, one way in which the length can be increased is by using spiral geometries [15, 16]. However, previous research has shown that spiral geometries are more susceptible to have a fundamental vibration mode that is torsional and, therefore, not ideal for vibrations energy harvesting [17]. Due to the resulting orthogonality of the electric field to the material polarization and placement of the electrodes, torsional strains are not readily harvestable by the flat rectangular profile of planar 2D beam shapes and are, therefore, undesirable [18]. Previously, a quad-folded spiral cantilever beam electromagnetic harvester was modelled using a finite element method (FEM), optimized to fit a $10 \times 10\,\text{mm}^2$ area, and shown to theoretically produce $2\,\mu\text{W}$ from 1 A of current in a wire [19]. This design, however, is susceptible to torsion due to the spiral-like design that as a result produces several strain nodes. The presence of strain nodes in the system require a more complex geometry for the placement of the electrodes as they need to be segmented to avoid a charge cancellation in order to increase the harvested power efficiency.

Recently, a zigzag geometry was proposed for energy harvesters as a means of reducing the natural frequency and maintaining a high power density when compared to a cantilever beam of similar dimensions [20, 21]. As with the spiral geometry, this design also experiences some torsion at its lower frequencies mainly due to the asymmetry of the design that results in lower efficiency. Interestingly, a zigzag design with a torsion-dominant fundamental mode was seen to produce more power than its bending-dominant second mode [22]. Symmetry has been applied to the zigzag design in [23, 24] in an effort to reduce the effect of torsion and subsequently produce a higher power output due to bending-dominant fundamental modes. The 'elephant' design mirrors a three-beam zigzag geometry along the length of the clamped beam and forms a closed connection at its free end [23]. This produced greater bending in the clamped beam where the highest amount of the strain is experienced. Their 25.4 mm by 25.4 mm harvester uses a piezoelectric layer on only the clamped beam to examine the reduced torsional effects and enhance pure bending for the fundamental mode. The elephant harvester was further able to combine the first two modes through mass loading structural modification and shown to produce more power than any of the considered mode shapes [25]. The 'meandering' design mirrors the zigzag geometry along the length of the free end [24]. Similarly, their 29 mm by 23 mm meandering design is shown to reduce torsion and experiences smaller shear strain at the anchor points. While the elephant and meandering designs show improvement in low frequency energy harvesting through base excitation, they use bulk PZT and are in the meso scale, and may be considered too large to be incorporated with microelectronics on a single-chip and too costly to mass produce. Reducing the overall footprint even further will potentially increase the resonant frequency but is required to allow for the realization of highly-scalable fabrication.
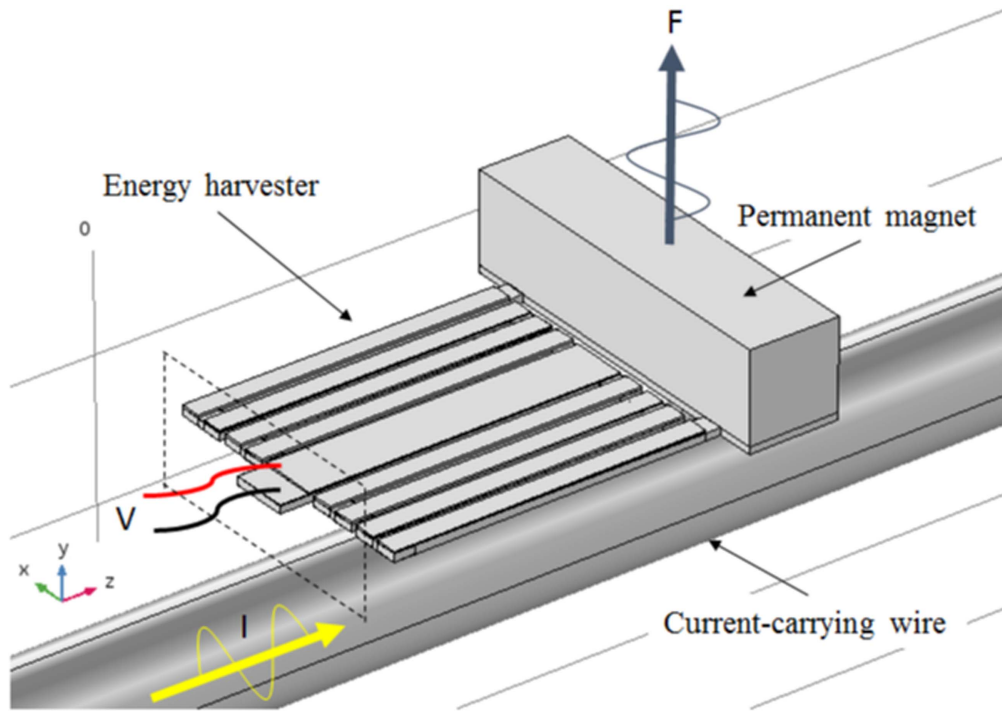
Figure 1. Schematic of a piezoelectromagnetic energy harvester on an AC-carrying wire.

The goal of the current work is to design a piezo-electromagnetic energy harvester that is fabricated using a low-cost screen-printing MEMS fabrication technique and alleviates some of the issues stated in the previous work in the literature. Screen-printed PZT thick films bridge the 1–100 μm gap between thin-film and bulk piezoelectrics, and allow for the creation of complex geometries like zigzags. PZT thick-films also make good candidates for MEMS energy harvesting applications since their coupling is higher than PZT thin-films. The proposed 12.7 mm by 14.7 mm centrally-supported meandering design has a low susceptibility to twist and experiences fewer strain nodes that remove complexities for the electrode fabrication. The harvester also employs PZT on every beam segment to increase the overall utilization of the footprint for harvesting. The unit is designed, fabricated, and tested for harvesting the electromagnetic energy from an AC current-carrying wire in North American transmission lines and, therefore, a resonant frequency of 60 Hz has been a major design criterion. A small footprint for the harvester was also desired to help with further integration of the unit with the sensor and wireless components in a single chip. Experimental displacement and voltage frequency response functions and measured power outputs as a function of current and distance from a wire are also presented and compared to the FEM results. Finally, the normalized power density of the current work is compared to various energy harvesters in the literature to highlight the advantage of the proposed design.
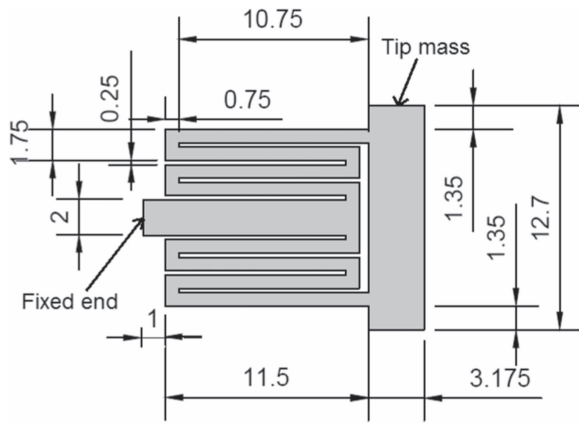
2. Piezoelectromagnetic energy harvesting working principle

Figure 1 illustrates the design and working principle of the piezoelectromagnetic energy harvester. The harvester is composed of a piezoelectric layer sandwiched between two electrodes on a metallic substrate with a permanent magnet attached to the tip. The harvester is mounted above an AC-carrying wire using a clamp where it is fixed at one end. The magnet couples to the alternating magnetic field produced by the wire. A sinusoidal electromagnetic force produced by the AC current around the wire excites the cantilever and causes the piezoelectric material to experience cyclic elastic deformation. Through the piezoelectric effect an AC voltage is generated across the electrodes that produces an electric current through the resistance load. The power produced can be calculated as the square of the root mean square (RMS) voltage across the load divided by its resistance. If the frequency of the electromagnetic force matches the resonant frequency of the harvester, the amplitude of the output power will be maximized as it results in a resonant condition.

The current-carrying wire emits a magnetic field according to the Biot–Savart law. The net force F_m on the magnet with flux density B_m can be described according to the following formula [26]

$$F_m = -B_m \oint_v \frac{d(H_x)}{dy} dV \tag{1}$$

where dV is the differential volume of the magnet and H_x is the x-component of the wire's magnetic field. Due to the unit's symmetric geometry and the symmetric positioning of the unit and the magnet above the wire, it is reasonable to assume that the motion will be primarily in bending and in the

Figure 2. Dimensioned (mm) schematic of energy harvester substrate.

Table 1. 301 Stainless steel properties.

Young's modulus	193 GPa
Density	7880 kg m^{-3}
Poisson's ratio	0.24
Thickness	0.254 mm

Table 2. Neodymium magnet (NdFeB, N42) properties.

Young's modulus	160 GPa
Density	7500 kg m^{-3}
Poisson's ratio	0.24
Dimensions	3.175 mm $\times$ 3.175 mm $\times$ 12.7 mm
Weight	0.96 g
Magnetic remanence	1.32 T

Table 3. Screen-printed PZT parameters.

Young's modulus	43 GPa
Density	5500 kg m^{-3}
Piezoelectric coefficient d$_{31}$	-40 pC N^{-1}
Thickness	0.075 mm

vertical direction, minimizing the possibility of a twist about the z-axis, or rotation about the y axis. Additionally, the electromagnetic force is purely translational and does not cause any rotation of the magnet about the x-axis. The magnet is also physically constrained to the substrate such that there is no rotation about the y-axis. Simply put, assuming small geometries, the force on the magnet is proportional to the current in the wire and inversely proportional to the square of the distance between the magnet and wire.

3. Design, modelling, and simulation

3.1. Design

The objective of the proposed geometry is to maximize the power density while maintaining a fundamental frequency in the range of 60 Hz to match the fundamental frequency of the North American power grid. A centrally-supported meandering (CSM) geometry is used in the current work and the proposed design is shown in figure 2. It is shown that this geometry achieves less torsion and bending becomes the dominant mode for the fundamental frequency. This results in higher energy harvesting efficiency. Furthermore, the geometry also minimizes the area of strain nodes that will be discussed in detail in the later section.

A permanent magnet is attached as a tip mass in the design to harvest energy from the electromagnetic field of the current-carrying wire and also to help tune the natural frequency of the system to the desired frequency. A neodymium magnet has been selected due to its strong magnetic flux density and availability in a variety of sizes. With respect to the piezoelectric material, PZT is chosen as it is known to have high coupling coefficients and allows for various available small-scale fabrication processes. For the proposed design, a screen-printed PZT technology is used as this process allows for fabrication of films in a 1–100 μm thickness range and also allows for fabrication of complicated geometries. The substrate of the system is 301-grade stainless steel. This substrate was selected for its relatively low Young's modulus and compatibility with the high firing temperatures

required during the fabrication process. Both the tip mass and the PZT are attached on the same side of the substrate. Finally, the geometry of the harvester also plays a significant role in achieving a low resonant frequency. A preliminary implementation of this device was first presented by the authors in [27].

The energy harvester has an overall footprint of 14.7 mm $\times$ 12.7 mm or 187 mm^2, which excludes the extra space near the clamp that is used for fine-tuning the resonant frequency. A 0.254 mm thick stainless steel substrate supports 75 μm thick strips of PZT on each beam. A fixed-end boundary condition is imposed by clamping one end of the central beam. The remainder of the structure is unrestricted and a neodymium magnetic proof mass is attached to the opposite end. The proposed geometry delivers nearly pure bending to the clamped beam where the majority of the stress is located. The proposed geometry also minimizes the area of strain nodes, which subsequently results in a greater harvestable area.

3.2. Modelling and simulation

The energy harvester is modelled using the 3D FEA software COMSOL Multiphysics and its associated MEMS module. The structural properties of the stainless steel and the neodymium magnet have been obtained from manufacturers [28, 29] and are presented in tables 1 and 2, respectively. Finally, the material properties of the screen-printed PZT were determined experimentally [30] and are presented in table 3.

The COMSOL software contains several default levels of meshing. Simulations were run with increasing levels of meshing until the incremental change in the resulting eigenfrequencies was below 1%. It was determined that the 'Fine'

Table 4. FEA meshing information.

Number of vertex elements	258
Number of edge elements	7891
Number of boundary elements	62 501
Number of elements	146 059

element mesh size was optimal as it provided the combination of solution convergence below the threshold and a reasonable simulation time. The meshing information for the final simulations is presented in table 4.

An eigenfrequency analysis is performed using the Solid Mechanics physics to obtain the natural frequency and mode shapes for the system. The eigenfrequency studies produce mode shapes that are independent of applied loads and are used to design the harvester to have a fundamental resonant frequency of 60 Hz. The corresponding mode shape is shown in figure 3.

The displacement mode shape shown indicates no noticeable torsion for the frequency of interest. As a result, each leg experiences pure compression or tension along its entire length during cyclic motion as shown in the strain plot in figure 5(a). This clearly demonstrates that one of the major design goals for reducing torsion in the fundamental mode of the system was achieved. The piezoelectric polarization plot is shown in figure 4(b) and areas of warm colors (red) indicate tension and positive charge whereas cold colors (blue) indicate compression and a negative charge production.

Additionally, in figure 4(a), it can be seen that there are no strain nodes. This is quite important as the presence of strain nodes will add complexities to the electrodes' configurations, as they need to be segmented in order to avoid charge cancellation. Also, there is an alternating strain pattern seen across adjacent beams of the system. The PZT outputs a voltage according to its strain profile and, therefore, a continuous electrode across the top and bottom of the entire structure cannot be used before polarization. Accordingly, the PZT has been placed along the length of each beam with disconnects at each beam link to avoid the strain nodes.

In order to obtain the frequency response functions (FRFs) for the displacement and voltage results, two separate COMSOL simulations are performed in the current work. First, the base excitation in the form of acceleration is provided to the clamped end of the harvester to obtain the displacement FRFs for output displacement divided by the base acceleration, similar to what is done in the experiments using shaker excitations for validation. The second simulation pertains to obtaining the voltage FRFs when the unit is operating in the real condition and mounted on the wire. For this purpose, an electromagnetic modelling is performed using a 2D model containing only cross-sections of the magnet and the wire to determine the electromagnetic force on the tip magnet due to the magnetic flux around the wire. The Magnetic Fields physics in COMSOL is used for this purpose. A 12.7 mm by 3.175 mm NdFeB magnet and an AWG10 wire with its conductor and insulation are modelled within a magnetically insulated space. A stationary study is performed to determine the electromagnetic force. The electromagnetic force from the 2D magnetic model is then multiplied by the depth of the magnet to obtain the total volumetric force on the magnet due to the current carrying wire. The calculated force is then applied to the bottom face of the magnet for the energy harvester model to obtain the voltage FRFs.

4. Geometry assessment

Before proceeding with fabrication, a study was performed to compare the power density of the centrally supported meandering geometry of the current work with the quad-folded (QF) spiral geometry proposed in [19]. The QF design is chosen over the meandering or elephant designs for comparisons to the proposed harvester due to the similarities for the intended application, i.e., harvesting from a current carrying wire. This allows for a fair comparison and serves to clearly highlight the advantages of the proposed design to better harvest from an AC current carrying wire. Specifically, the purpose of the study was to confirm the energy harvesting
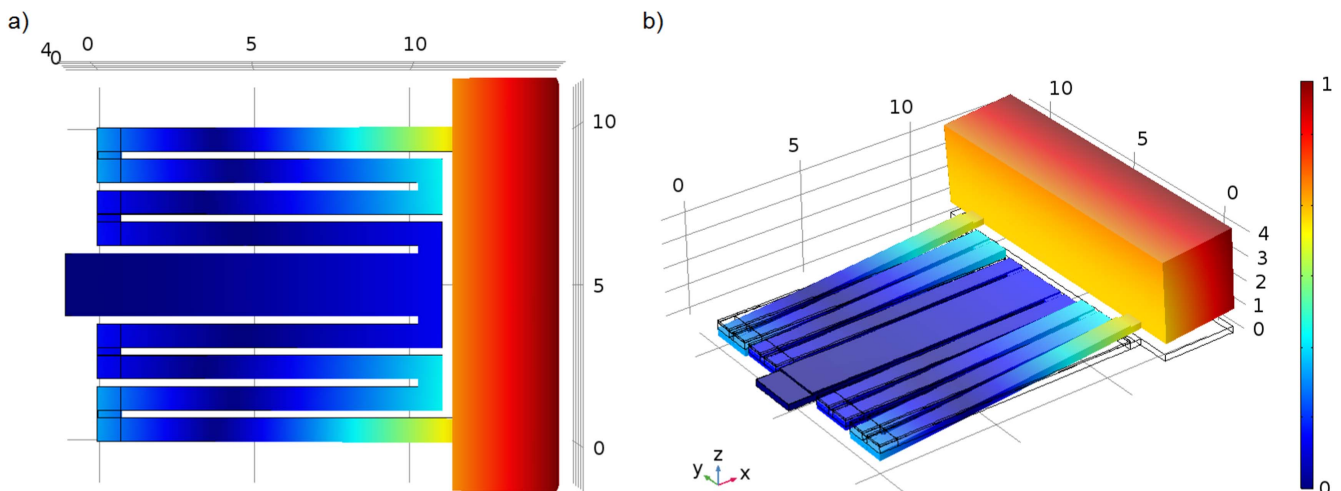
Figure 3. Fundamental mode shape showing total displacement (mm) (a) Top view. (b) Isometric view.
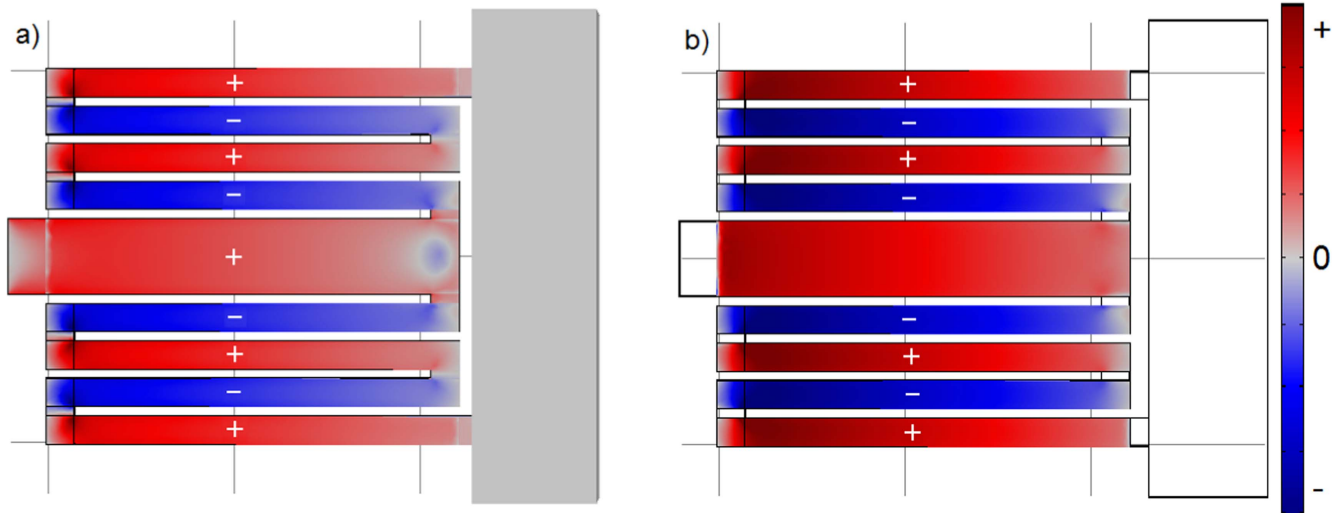
Figure 4. Fundamental mode shape (a) Strain. (b) Piezoelectric polarization.

advantages of the proposed geometry while minimizing the impact of other contributing factors such as piezoelectric material, footprint, tip mass, and magnetic properties.

As shown in figure 5, the QF cantilever design studied in [19] utilizes four beams that are folded around in a spiral shape, and attach to a central mass at the end. In this design, the entire length of each beam contains a piezoelectric layer. The geometry contains four fixed constraints, one in each end corner, and the central tip mass acts like a guided end due to a symmetric geometry. A COMSOL stress analysis for this structure shows that each beam segment experiences both tension (red) and compression (blue), and indicates that large areas exist where very little strain (grey) is experienced. These areas pertain to the strain node sections where power harvesting has minimal efficiency. The combination of both tension and compression in a single beam segment requires complicated electrode patterning for energy harvesting to ensure minimal voltage cancellation. These large strain nodes are left without electrodes. Moreover, due to the spiral shape, the structure experiences torsional stresses, which are not readily harvestable.

The CSM geometry proposed in this study is a fixed-free folded design similar to a cantilever, shown in figure 6. The central beam is clamped at one end and extends into a zigzag pattern that wraps around to form a closed loop which supports a tip mass. Similar to a cantilever beam, this structure experiences the greatest amount of strain near its clamped end. The symmetry of this design reduces torsion in the beams, which results in greater bending effects and a more efficient energy harvester. Each beam supports a layer of piezoelectric material, and contains a small disconnect between each beam segment to allow for individual polarization or electrodes. Important to note is that each beam segment experiences either tension or compression. This permits a single continuous electrode for each beam, allowing for full utilization of the piezoelectric material and removes the need for segmented electrodes to avoid a charge
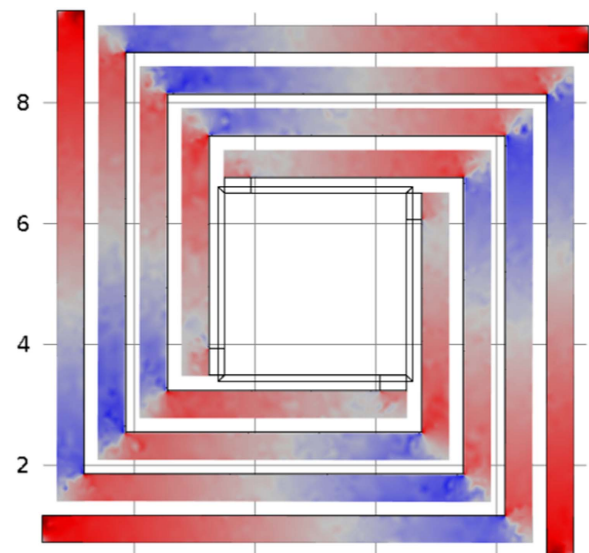

**Figure 5.** Quad-folded (QF) cantilever strain plot.

cancellation. This is a major advantage for the screen-printing fabrication.

The QF geometry is compared with variations of the CSM geometry shown in figure 6 to determine the best geometry for the piezoelectromagnetic energy harvester. These designs are modelled using COMSOL for their power output comparison. PZT-5A and a silicon substrate are chosen for this analysis for all designs. The same dimensions and magnetic properties are used for the tip mass in all cases. Also, the designs shown in figure 7 have similar footprints to that of the QF design to ease the comparisons. Eigen-frequency and frequency response analyses are performed to determine the resonant frequency and power output per footprint using the optimal load for each case. A wire current of 1 A and a distance of 4 mm are used and the results of the simulations are presented in table 5.

The results from the study show that both CSM designs produced larger power and had at least three times more
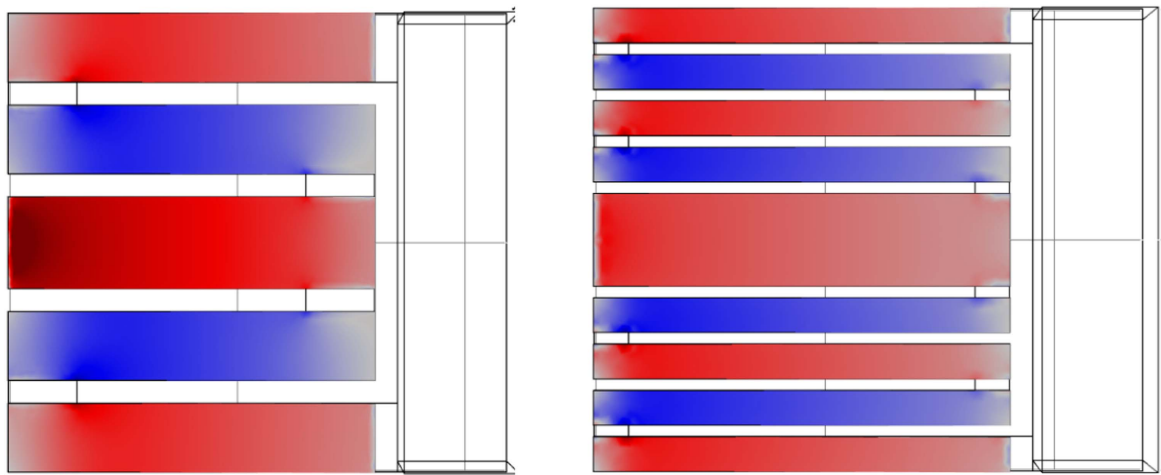
Figure 6. Centrally supported meandering geometry with 5 beams (left) and 9 beams (right). The unit is fixed at the left side of the center beam.
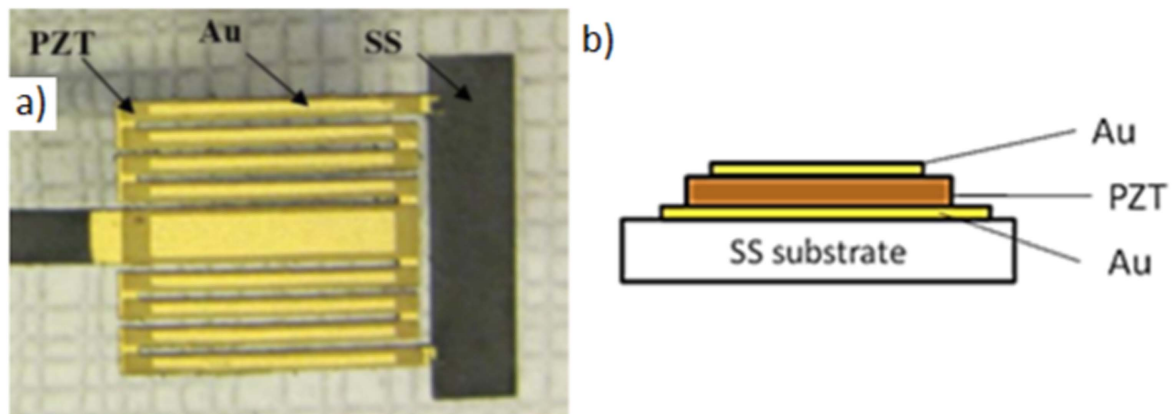
Figure 7. Piezoelectromagnetic energy harvester fabricated using screen-printing technology (a) Top view. (b) Cross-sectional schematic of one beam.

Table 5. Comparison of quad-folded and two centrally-supported meandering designs.

	Quad-folded	9 Beams	5 Beams
Eigenfrequency (Hz)	56.53	56.39	56.61
Optimal load, R_l (Ω)	10 000	50 000	10 000
Frequency @ R_l (Hz)	56.53	56.58	57.82
Power @ R_l (μW)	3.1	11.2	11.8
Footprint (mm^2)	$10 \times 10 = 100$	$11.88 \times 10 = 119$	$10 \times 10.5 = 105$
Power/footprint (uW mm^{-2})	0.031	0.094	0.112
Force on magnet (N)	0.000 26	0.000 26	0.000 26
Number of fixed constraints	4	1	1
PZT thickness (μm)	1	181	62
Area of PZT, AP (mm^2)	39	72	64
Area of electrodes, AE (mm^2)	21	72	64
AE/AP	54%	100%	100%
Power/active area	0.15	0.16	0.18

power per footprint area. The optimal loads of the designs were found to be in the 10 kΩ range. For fair comparison, all units have been designed to have the same fundamental frequencies. Since the CSM designs have fewer fixed constraints and therefore are more flexible than the QF cantilever, the thickness of the PZT is found to be larger for these designs to tune to the same fundamental frequency. This subsequently allows for a higher energy harvesting efficiency. Furthermore, the CSM designs also offer a greater harvestable area (area of the electrodes, AE, divided by the area of PZT, AP) with less

strain node areas, a greater active area for PZT, and even a greater power output per active area. For the reasons mentioned, the CSM was further optimized as described in the previous section and chosen for this application. Finally, the proposed unit and its symmetricity around the fixed ends allows for a design that is less susceptible to the torsional modes.

5. Fabrication

The materials used in the fabrication process consist of a stainless steel substrate, thin gold electrodes, and PZT. The stainless steel substrate was laser cut (KJ Laser Micromachining) according to the designed geometry. Stainless steel was selected as a substrate for its compatibility with the high firing temperature required by the screen-printing process and for its flexibility when compared with the alumina substrates normally used with thick films. Commercially available gold ink (ESL8836 from ElectroScience Laboratories) is used for the electrode layers, whereas the PZT is prepared at the IMS laboratory [31, 32].

A DEK HORIZON 03iX machine is used for the printing process, and a specially built structure holds the substrate during all levels of printing. The bottom gold electrode, PZT layer, and top gold electrode are successively printed and dried at $120\,^{\circ}\mathrm{C}$ using $325\,\mu m$, $200\,\mu m$, and $325\,\mu m$ mesh screens, respectively. The dried samples then undergo hot isostatic pressing to reduce the porosity of the PZT, thus improving the material's electromechanical properties. Afterwards, the samples are co-fired for two hours at $900\,^{\circ}\mathrm{C}$ in air atmosphere and an optical profiler found the PZT thickness to be approximately $75\,\mu m$. Figure 7 shows the fabricated unit after firing and a schematic of the unit cross-section.

The next step of the fabrication is the polarization of the PZT layers to exhibit piezoelectric properties. A strain-matched polarization scheme is used to mitigate voltage cancellation across the harvester [24]. The PZT of each beam is poled such that each adjacent member has the opposite poling direction to match the strain plots in figure 4(a). Beams of the same strain were first micro-wired together using a ball-bonding technique. Then both positive and negative groups were polarized by applying $0.250\,\mathrm{kV}$ for $10\,\mathrm{min}$ at $280\,^{\circ}\mathrm{C}$ under nitrogen according to the sign of figure 4(a). By employing this approach, all of the electrodes have the same voltage polarity under strain. After poling, micro-wire connections are made between the top electrodes of all the beams. This allows for a single continuous electrode to be used across the bottom layer of the energy harvester. Finally, the magnet is glued to the tip of the substrate using a thin layer of epoxy and left to cure for two days. The completed energy harvester is shown in figure 8.
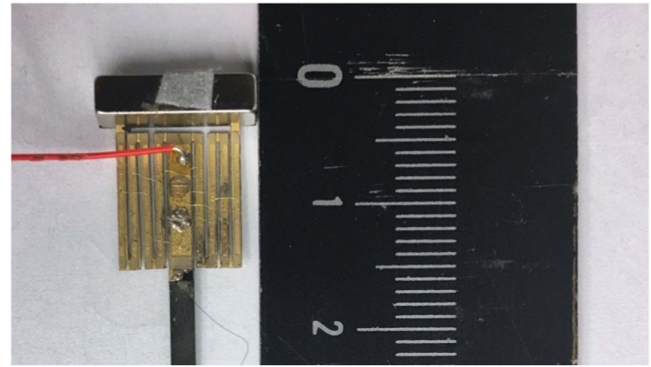

Figure 8. Fabricated energy harvester with magnet.

6. Experimental results

Experimental results are obtained to validate the COMSOL model. It should be noted that the COMSOL model assumes an excitation force with constant magnitude whereas experimentally the force on the magnet varies as the harvester undergoes vibrations. Therefore, experiments are used to assess the validity of this assumption for the range of the current values used for this work.

6.1. Shaker test—no tip mass

To validate the COMSOL model the fabricated unit was experimentally tested. Initially, a shaker was used as the excitation source for the energy harvester to validate the dynamic behavior of the system. As a preliminary step, the energy harvester is tested prior to affixing the magnet. This minimizes the introduction of errors from the process of epoxying the tip magnet and provides a simpler case for comparison to the COMSOL results.

Figure 9 shows the test setup used to obtain the displacement FRFs of the energy harvester. A Modal Shop 2075E dual-purpose electrodynamic shaker is used to excite the energy harvester using a base excitation. An LMS SCADAS mobile data acquisition system is used to control the shaker, and to perform a frequency sweep analysis using the Sine Control module. The sinusoidal input signal is amplified through a Modal Shop 2050E09 power amplifier. An accelerometer is mounted on the shaker to provide controlled feedback during the frequency sweep and maintain the desired acceleration. During excitation, a Polytec OFV-505 laser vibrometer and OFV-5000 controller are used to measure the tip displacement. An additional distance of $3\,\mathrm{mm}$ from the clamp is used in the experimental tests to reduce the stress experienced in the PZT near the clamp and minimize chances for damage to the harvester.

A frequency sweep from $30\,\mathrm{Hz}$ to $500\,\mathrm{Hz}$ with an input acceleration of $0.2\,g$ was performed to capture the first three modes, and the displacement FRFs of the experimental and simulation results are shown in figure 10. A sweep rate of $0.1\,\mathrm{Hz\,sec^{-1}}$ was used to obtain the FRFs and was slowed down near resonance peaks. The slow sweep rate and the low acceleration level used for this validation reduce the presence of nonlinearities in the response, and allow for a fair
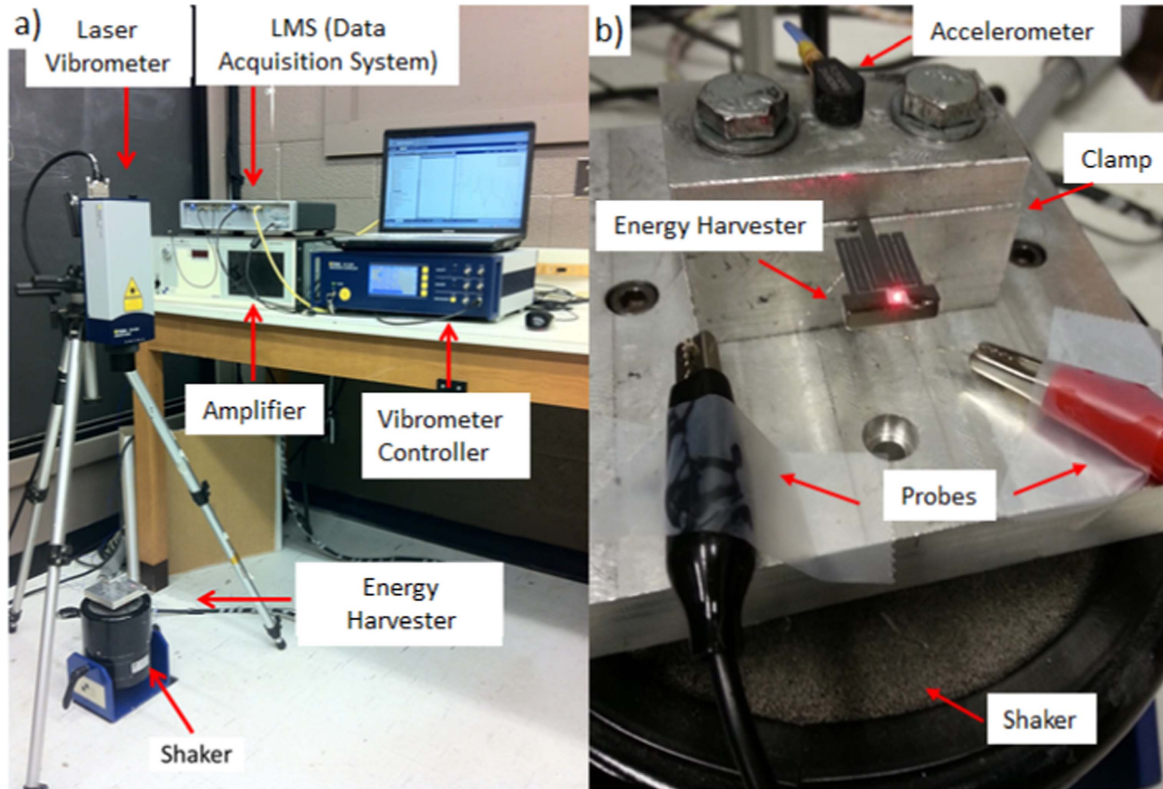
Figure 9. (a) Experimental test setup equipment. (b) Close up of EH.

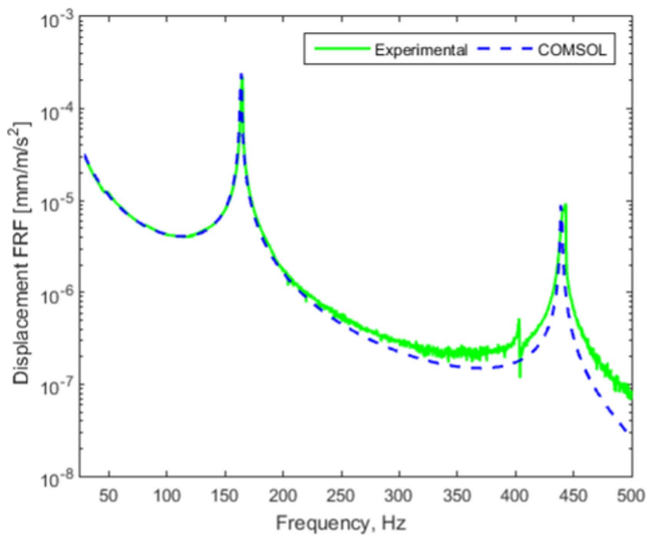**Figure 10.** Experimental and model displacement FRFs of the energy harvester without a tip mass.

Figure 11. Experimental and model displacement FRFs of the energy harvester with a tip mass.

comparison with the discrete steady-state responses from the COMSOL model. The displacement measurement is performed at the center of the tip of the harvester as also shown as a laser target in figure 9(b).

Experimentally, the first two bending modes occur at 164.75 Hz and 443 Hz, and the first torsional mode occurs at 403.25 Hz. COMSOL predicts the first two bending modes at 163.61 Hz and 439.38 Hz, errors of less than 1%. COMSOL predicts the first torsional mode at 401.24 Hz, an error of 0.5%. The torsional mode for the COMSOL model does not
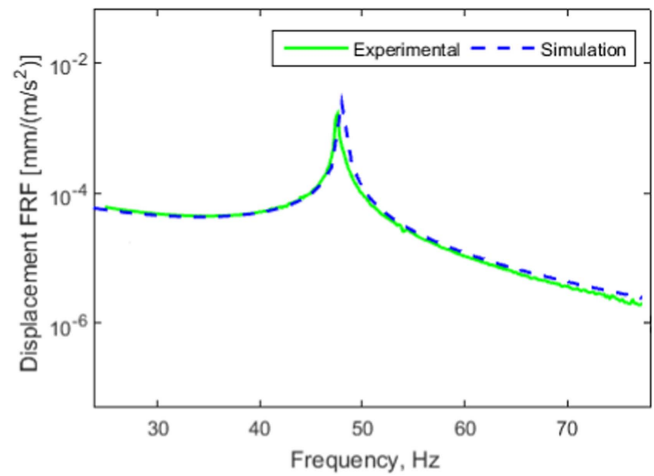
appear in the displacement FRF of figure 10 because the sensing point is chosen exactly in the center of the tip mass area. Due to symmetry the torsional mode is not seen at this centerline but the frequency is taken from the eigenfrequency analysis. Also in figure 10 it is seen that there is a good agreement in the amplitudes for the displacement FRFs when comparing experimental and simulation results that further validates the model as a viable tool for future optimization.
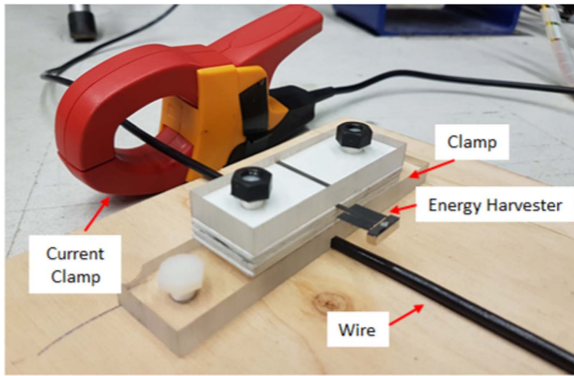
Figure 12. Experimental test setup of the piezoelectromagnetic energy harvester on a current-conducting wire.
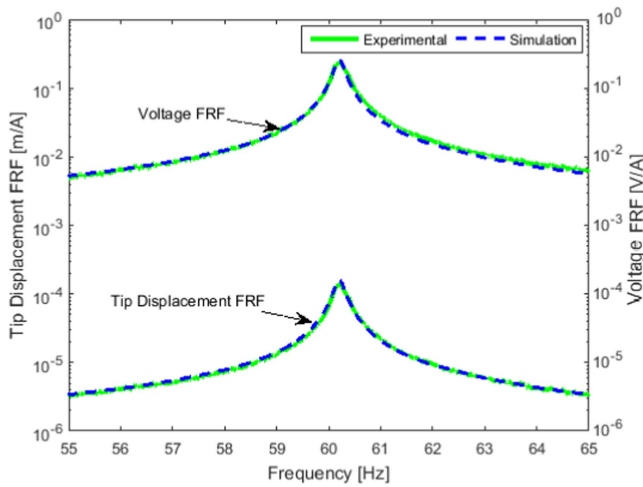

Figure 13. Tip displacement and voltage FRFs showing a resonant frequency at 60.3 Hz (wire current = 1 A at a distance of 12.5 mm).
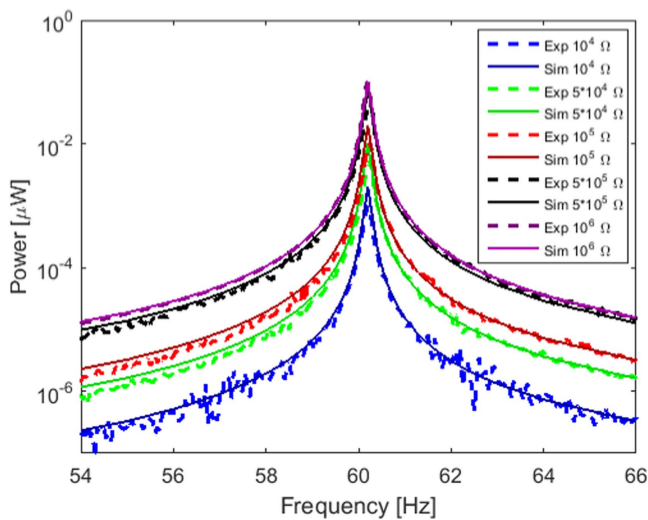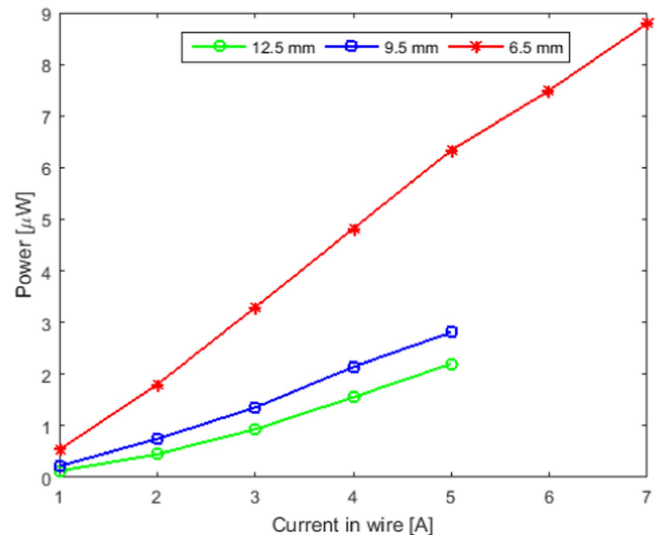

Figure 14. Power curves across 10 kΩ to 1 MΩ resistive loads (wire current = 1 A at a distance of 12.5 mm).

6.2. Shaker test—tip mass included

Next, the magnetic tip mass is epoxied to the harvester and the displacement FRF is obtained. Since the fundamental
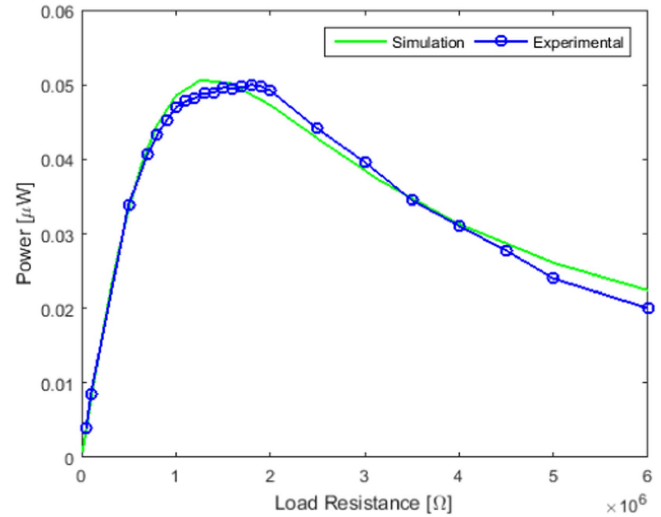

Figure 15. Power output with respect to load resistance (Wire current = 1 A at a distance of 12.5 mm).

Figure 16. Power output as a function of electric current and distance from wire for the optimal load.

frequency provides the greatest power output from the energy harvester, and considering the good match in the results without a tip mass, the frequency sweep is performed for the 25 Hz–80 Hz that embraces the first peak. An input acceleration of 0.2 g was used. The experimental and simulation FRFs are presented in figure 11.

In figure 11 the experimental fundamental frequency is measured to be about 47.6 Hz and the COMSOL result is 48.1 Hz, an error of 1%. The experimental fundamental frequency of 47.6 Hz being lower than the design requirement 60 Hz is due to the additional 3 mm distance used from the clamp to minimize potential damage to the unit. This was fixed later when the unit was tested on the wire to attain the desired frequency of 60 Hz. Furthermore, figure 11 indicates that the amplitudes of the displacement FRFs match very well. This indicates that the COMSOL model accurately
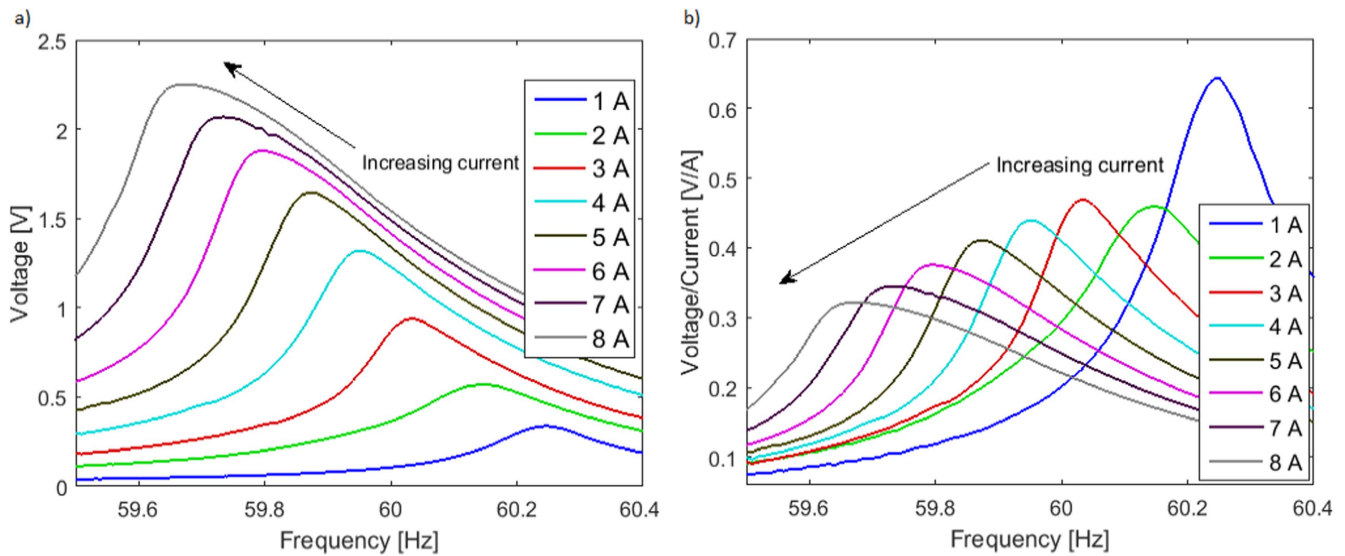
Figure 17. Voltage frequency responses for increasing wire currents demonstrating nonlinear effects (d = 6.5 mm) (a) Voltage amplitude. (b) Voltage FRF.

predicts the dynamic behavior of the proposed energy harvester design.

6.3. Wire test

The final experimental tests were performed on a unit using a wire excitation using the setup shown in figure 12. The unit was mounted above a 10 AWG current-carrying wire using an acrylic base and 1.5 mm thick spacers to control the distance between the magnet and the wire. The vertical distance between the magnet and wire was measured using a plastic caliper. An LMS SCADAS mobile data acquisition system is used to control the current amplitude and frequency in the wire and to perform a frequency sweep analysis using the Sine Control module. A Fluke i400s AC clamp is used to provide the feedback control for the wire's current amplitude. It should be noted that for model validation purposes the setup is used to measure the voltage and displacement FRFs for the unit for an input electric current through the wire of a constant magnitude that is swept across a range of frequencies and controlled using the sine sweep module. Therefore, the sine sweep electric current signal does not have a 60 Hz dominant frequency, and the peaks shown further in the FRF plots indicate the natural frequency of the unit after the previously used 3 mm gap to avoid damages during the vibration testing was removed. A similar arrangement is generally adopted for modal analysis and testing where the system is provided with a constant mechanical input in the form of displacement or acceleration across a range of frequencies instead of an excitation of a given frequency. The output voltage produced by the system is measured by the LMS system with an input impedance of 1 MΩ using a 10:1 probe. Any resistive load is adjusted to account for the 10 MΩ input resistance. The frequency resolution of the data acquisition is 0.01 Hz.

The harvester was initially tested with a relatively low input force (both low current and high distance from wire) to minimize the presence of nonlinear effects. The harvester was mounted above the wire at a distance of 12.5 mm between the bottom of the magnet and the top surface of the wire carrying a 1 A current using a sine sweep signal over the range of frequencies shown in figure 13. The experimental and simulated tip displacement and open-circuit voltage FRFs for a range of 55 Hz to 65 Hz are shown in figure 13.

The experimental and simulated results show a strong agreement in both the amplitude and resonant frequency. This indicates that the COMSOL model accurately predicts the dynamic behavior of the proposed energy harvester design. The experimental resonant frequency was found to be 60.3 Hz that is suitable for harvesting from the North American power grid. It should be noted that this frequency was tuned by adjusting the distance from the clamp. The COMSOL model predicted a resonant frequency of 60.2 Hz, which shows a negligible error. The damping ratio is calculated by using the quadrature peak picking method [33]. The damping ratio zeta was found to be approximately 0.0027 from the voltage FRF test results and applied to the COMSOL model.

6.4. Load sweep

Next, the energy harvester is tested with different resistive loads to determine the optimal load resulting in the maximum power transfer. An Elenco resistor substitution box is used to conveniently provide the numerous resistances. The power is calculated by using the square of the measured RMS voltage across a resistor and dividing by its resistance value ($P_{ave} = V_{RMS}^2/R_{load}$). The power outputs across 10 kΩ to 1 MΩ are shown in figure 14.

No noticeable shift in resonant frequency is seen across the load sweeps. The difference in power output between the 500 kΩ and the 1 MΩ loads appears small, with the 1 MΩ resistor resulting in the highest power output. This shows that the resistor values resulting in the greatest power transfer are in this proximity. The simulation and test results are shown to

Table 6. Normalized power density for previous piezoelectromagnetic harvesters and the present work.

Reference	Deposition method	Magnet distance (mm)	Magnetic remanence (T)	Wire current (A)	Power output (μW)	Frequency (Hz)	Effective volume (mm^3)	Normalized power density μW/(T[a] A[a] mm)
The present design	Screen-printed PZT	6.5	1.32	7	9	60	169.7	0.243
Paprotny [19]	Sputtered AlN	2.5[a]	1.32	1	2 (simulated)	57[a]	111.81	0.085
Olszewski [14]	Sputtered AlN	2[a]	1.3	2	1.5	42.3	20.69	0.112
Paprotny [6]	Bulk PZT	2.5	1.48	20	2700	60	1731.06	0.329
Chen [8]	Bulk PZT	2	1.4[a]	2.5	295.3	50	1282.74[a]	0.263
He [7]	Bulk PMgN-51	4	1.45	10	566	50	265.92	2.349

[a] Values interpolated from data in the referenced literature.

be in excellent agreement. To obtain the final optimal value for the load resistance, the power plot is produced for the optimal range found in figure 14 and is shown in figure 15. An area of the plot between approximately 1 MΩ to 2 MΩ, the optimal range, shows small variation (less than 5%) in power production and can serve as the optimal load resistance.

6.5. Power output versus the current and distance to the wire

With the electromechanical model experimentally validated and the optimal load resistance range determined, the power outputs were measured using various distances to the wire and various electric current values. Figure 16 shows the experimental power outputs measured across a 1 MΩ resistive load as a function of current and distance to the wire for the harvester.

It is shown that at a distance of approximately 6.5 mm to a wire carrying a 7 A current, approximately 9 µW is dissipated across the 1 MΩ load. Since the force on the magnet is inversely proportional to the square of the distance and the power output is proportional to the square of the force, the overall power output grows significantly as the distance between the magnet and wire are minimized. Under large forces, however, nonlinear effects become more evident and result in a lower experimental power than expected. Further tests at smaller distances and larger current values were voided to prevent damage to the unit during these vibrations.

6.6. Nonlinear effects

As the current in the wire increases, equation (1) predicts a larger total force on the magnet. This leads to larger displacements in the system and, consequently, the open-circuit voltage output will increase. This behavior is observed in figure 17(a), which presents the experimental open-circuit voltage output of the energy harvester for various wire currents, increasing in 1 A increments from 1 to 8 A. In addition to the increase in voltage output, it is observed in figure 17(a) that the resonant frequency decreases as the wire current increases. It is also observed that the peak frequencies are shifted to the left for the higher current values. This indicates of some nonlinear effects that should be investigated further through careful observation of the output-input ratios-FRFs.

The experimental voltage FRFs presented in figure 17(b) also demonstrate a decrease in both the voltage FRF peak value and the resonant frequency as the wire current increases. These effects are attributable with varying degrees to a decrease in the quality factor and the stiffness of the unit (some softening effects) occurring as the wire current increases and the unit experiences overall larger displacements during its vibrations [34]. Additionally, variations of the magnetic forces experienced by the unit as its distance to the wire changes during these oscillations can be partially a cause for this. Although further testing is required to truly quantify the nonlinear effects and their potential sources, these results serve to highlight the importance that, for a given application, the input force must be considered when tuning

the energy harvester to a specified frequency. Finally, it is seen in figure 17 that a larger harvesting frequency bandwidth is obtained with increasing excitation force.

6.7. Comparisons to other works

In this section, the results of the proposed design are compared to the previous work in the literature and presented in table 6. As previously mentioned, the overall power output is a function of the current in the wire, the distance between the magnet and the wire, and the remanence of the magnets. Therefore, all of these must be considered for a fair comparison. The effective volume considers the sum of the volume of all beams and magnets. The normalized power density of the piezoelectromagnetic energy harvesters is calculated by dividing the power output by both the effective volume and the magnetic force.

By comparing the normalized power densities shown in the table, one can see that the present work shows significant improvement over previous MEMS devices, [19] and [14], with a 2.9 and 2.2 times increase in the normalized power density, respectively. This improvement validates the advantages of the centrally-supported meandering geometry and the screen-printing fabrication process. The proposed geometry minimizes the number of overall strain nodes that plague other geometries. The results for the present work also show good potential when compared to the larger scale units in [6–8]. Additionally, in these larger scale devices, bulk PZT is used and is known to have higher electromechanical coupling compared to the MEMS fabricated technology, and, therefore, is expected to have higher normalized power densities. As such, the benefits of the MEMS screen-printing fabrication technology remains one of the main advantages of the present work. Also, it is seen that the result of the proposed design is quite comparable to that of the bulk PZT units for [6], [8].

7. Conclusion

A MEMS piezoelectromagnetic energy harvester has been fabricated through screen-printing of PZT on a stainless steel substrate with a centrally-supported meandering geometry. The unit is used to harvest electrical energy in a non-invasive manner from the transmission lines to help power the sensors for a smart grid. The device is modelled using COMSOL, and validated against its experimental results for the displacement and power frequency response functions. The natural frequency design requirement is chosen as 60 Hz to match the fundamental frequency of the current in transmission lines. It is shown that the proposed geometry experiences dominant bending when compared to the previous MEMS-based work on this technology, helps increase the power efficiency, and simplifies the electrode geometry. As a result, the present work results in an improved normalized power density compared to the previous MEMS-based piezoelectromagnetic harvesting technologies for the proposed application.

Currently, work on integrating the energy harvester with power conditioning and wireless communications circuitry is

in progress [32]. The ultimate goal is to combine the harvester, circuitry, and a current sensor into a single chip to obtain a self-contained sensing solution for transmission power lines. Future work will also involve improving the fabrication process to provide a refined poling process to remove complicated wiring and may reduce the overall damping.

Acknowledgments

ORCID iDs

Armaghan Salehian https://orcid.org/0000-0001-5032-4124

References

[1] Naifar S, Bradai S, Viehweger C and Kanoun O 2017 Survey of electromagnetic and magnetoelectric vibration energy harvesters for low frequency excitation *Measurement* **106** 251–63

[2] Leland E, Wright P and White R 2007 Design of a MEMS passive, proximity-based AC electric current sensor for residential and commercial loads *PowerMEMS* 77–80

[3] Lao S B, Chauhan S S, Pollock T E, Schröder T, Cho I S and Salehian A 2014 Design, fabrication and temperature sensitivity testing of a miniature piezoelectric-based sensor for current measurements *Actuators* 162–81

[4] Leland E S, White R M and Wright P K 2006 Energy scavenging power sources for household electrical monitoring *PowerMEMS Proc. 6th Int. Workshop Micro Nanotechnol. Power Generat. Energy Convert. Appl.* pp 165–8

[5] Pollock T 2014 Design, modelling, fabrication & testing of a miniature piezoelectric-based EMF energy harvester *Master's Thesis* University of Waterloo

[6] Paprotny I, Xu Q, Chan W W, White R M and Wright P K 2013 Electromechanical energy scavenging from current-carrying conductors *IEEE. S. J.* **13** 190–201

[7] He W, Li P, Wen Y, Zhang J, Lu C and Yang A 2013 Energy harvesting from electric power lines employing the Halbach arrays *Rev. Sci. Instrum.* **84** 105004

[8] Chen W, Cao Y and Xie J 2015 Piezoelectric and electromagnetic hybrid energy harvester for powering wireless sensor nodes in smart grid *J. Mech. Sci. Technol.* **29** 4313–8

[9] Clement P, Perez E D C, Gonzalez O, Calavia R, Lucat C, Llobet E and Debéda H 2016 Gas discrimination using screen-printed piezoelectric cantilevers coated with carbon nanotubes *Sens. Actuators* B **237** 1056–65

[10] Katsumura H 2017 Development of piezoelectric vibration energy harvesters for battery-less smart shoes *PowerMEMS 2017: 17th Int. Conf. on Micro and Nanotechnology for Power Generation and Energy Conversion Applications*

[11] Xu R, Lei A, Dahl-Petersen C, Hansen K, Guizzetti M, Birkelund K, Thomsen E V and Hansen O 2012 Screen printed PZT/PZT thick film bimorph MEMS cantilever device for vibration energy harvesting *Sens. Actuators* A **188** 383–8

[12] Costache F, Pawlik B and Rieck A 2017 Development of a compact, low-frequency vibration, piezoelectric MEMS energy harvester *Multidisciplinary Digital Publishing Institute Proceedings* 588

[13] Roundy S and Wright P K 2004 A piezoelectric vibration based generator for wireless electronics *Smart Mater. Struct.* **13** 1131

[14] Olszewski O Z, Houlihan R, Mathewson A and Jackson N 2016 A low frequency MEMS energy harvester scavenging energy from magnetic field surrounding an AC current-carrying wire *J. Phys.: Conf. Ser.* **757** 012039

[15] Ibrahim M and Salehian A 2015 Modeling, fabrication, and experimental validation of hybrid piezo-magnetostrictive and piezomagnetic energy harvesting units *J. Intell. Mater. Syst. Struct.* **26** 1259–71

[16] Monin T, Tessier-Poirier A, Léveillé E, Juneau-Fecteau A, Skotnicki T, Formosa F, Monfray S and Fréchette L 2016 First experimental demonstration of a self-oscillating fluidic heat engine (SOFHE) with piezoelectric power generation *J. Phys.: Conf. Ser.* 012039

[17] Karami M A, Yardimoglu B and Inman D J 2010 Coupled out of plane vibrations of spiral beams for micro-scale applications *J. Sound Vib.* **329** 5584–99

[18] Karami M A and Inman D J 2012 Parametric study of zigzag microstructure for vibrational energy harvesting *J. Microelectromech. Syst.* **21** 145–60

[19] Paprotny I, White R and Wright P 2010 Modeling, design and fabrication of ($10 \times 10 \times 4$ mm^3) MEMS AC energy scavenger for smart grid applications *Proc. 10th Int. Workshop Micro Nanotechnol. Power Generat. Energy Convert. Appl.* pp 107–10

[20] Karami M A and Inman D J 2011 Analytical modeling and experimental verification of the vibrations of the zigzag microstructure for energy harvesting *Journal Vib. Acoust.* **133** 011002

[21] Sharpes N, Abdelkefi and Priya S 2014 Comparative analysis of one-dimensional and two-dimensional cantilever piezoelectric energy harvesters *Energy Harvesting and Systems* **1** 209–16

[22] Abdelmoula H, Sharpes N, Abdelkefi A, Lee H and Priya S 2017 Low-frequency Zigzag energy harvesters operating in torsion-dominant mode *Appl. Energy* **204** 413–9

[23] Sharpes N, Abdelkefi A and Priya S 2015 Two-dimensional concentrated-stress low-frequency piezoelectric vibration energy harvesters *Appl. Phys. Lett.* **107** 093901

[24] Berdy D F, Srisungsitthisunti P, Jung B, Xu X, Rhoads J F and Peroulis D 2012 Low-frequency meandering piezoelectric vibration energy harvester *IEEE Trans. Ultrason. Ferroelectr. Freq. Control* **59** 846–58

[25] Sharpes N, Abdelkefi A and Priya S 2016 Mode shape combination in a two-dimensional vibration energy harvester through mass loading structural modification *Appl. Phys. Lett.* **109** 033901

[26] Wagner B, Kreutzer M and Benecke W 1993 Permanent magnet micromotors on silicon substrates *J. Microelectromech. Syst.* **2** 23–9

[27] Fernandes E, Zarabi S, Debéda H, Lucat C, Nairn D, Wei L and Salehian A 2016 Modelling and fabrication of a compliant centrally supported meandering piezoelectric energy harvester using screenprinting technology *J. Phys.: Conf. Ser.* **773** 012109

[28] AK Steel www.aksteel.com

[29]   K&J Magnetics www.kjmagnetics.com

[30]   Castille C 2010 Etude de MEMS piézoélectriques libérés et microstructurés par sérigraphie.Application à la détection en milieu gazeux et en milieu liquide *PhD Thesis* Université de Bordeaux

[31]   Debéda H, Clément P, Llobet E and Lucat C 2015 One-step firing for electroded PZT thick films applied to MEMS *Smart Mater. Struct.* **24** 025020

[32]   Debéda H, Rua-Taborda I, Fernandes E, Zarabi S, Nairn D, Wei L and Salehian A 2017 Printed MEMS-based self– contained piezoelectric-based monitoring device for smart grids *PowerMEMS 2017: 17th Int. Conf. on Micro and Nanotechnology for Power Generation and Energy Conversion Applications*

[33]   Inman D J 2014 *Engineering Vibration* (Upper Saddle River, NJ: Pearson)

[34]   Shen D, Park J, Ajitsaria J, Choe S, Wikle H C III and Kim D 2008 The design, fabrication and evaluation of a MEMS PZT cantilever with an integrated Si proof mass for vibration energy harvesting *J. Micromech. Microeng.* **18** 055017